Arabian Journal of Chemistry (2019) **12**, 1298–1307

King Saud University

Arabian Journal of Chemistry

www.ksu.edu.sa
www.sciencedirect.com

SPECIAL ISSUE: ENVIRONMENTAL CHEMISTRY

Catalytic wet air oxidation of phenol over ultrasound-assisted synthesized Ni/CeO_2–ZrO_2 nanocatalyst used in wastewater treatment

Mohsen Parvas, Mohammad Haghighi *, Somaiyeh Allahyari

Chemical Engineering Faculty, Sahand University of Technology, P.O. Box 51335-1996, Sahand New Town, Tabriz, Iran
Reactor and Catalysis Research Center (RCRC), Sahand University of Technology, P.O. Box 51335-1996, Sahand New Town, Tabriz, Iran

Received 12 July 2013; accepted 22 October 2014
Available online 18 November 2014

KEYWORDS

Ni/CeO_2–ZrO_2;
Sonochemistry;
Precipitation;
Nanocatalyst;
CWAO;
Phenol

Abstract Non-noble metal Ni with different loadings was coated on precipitated CeO_2–ZrO_2 support by the sonochemistry method and examined for catalytic wet air oxidation of phenol. The structure of the nanocatalysts was determined by BET, FESEM, XRD, and FTIR analyses. The results showed non-uniform morphology of the nanocatalyst at lower Ni contents changed to homogenous morphology with spherical nano particles at higher Ni contents. While the size of NiO crystals remained constant with rising Ni content, the crystallinity of NiO significantly increased. If the crystallinity of NiO was 100% in 20% wt Ni/CeO_2–ZrO_2, the crystallinity of NiO in 5% wt Ni was found to be 41.13%. The average particle size in Ni(15%)/CeO_2–ZrO_2 was 77 nm in which 85.71% of particle diameters were less than 100 nm. Catalytic wet air oxidation of phenol with different Ni loadings indicated improvement of phenol destruction at higher amounts of active phase. Removal of phenol increased with increasing catalyst loading from 4 to 9.0 g/l but further increase to 10 g/l declined the catalyst reactivity.

1. Introduction

As a result of stricter environmental regulations, wastewater treatment has become a major issue (Besson et al., 2000). Many wastewaters originating from chemical, pharmaceutical and petrochemical industries have phenol contaminations (Lin et al., 2003), conferring a heavy burden to the environment. Phenol and its derivatives are known to be detrimental to human health and aquatic life and they will give water a particularly disagreeable taste and odor even at concentrations below 0.001 mg/l (Pintar and Levec, 1994).

* Corresponding author at: Chemical Engineering Faculty, Sahand University of Technology, P.O. Box 51335-1996, Sahand New Town, Tabriz, Iran. Tel.: +98 413 3458096, +98 413 3459152; fax: +98 413 3444355.
E-mail address: haghighi@sut.ac.ir (M. Haghighi).
URL: http://rcrc.sut.ac.ir (M. Haghighi).
Peer review under responsibility of King Saud University.

Production and hosting by Elsevier

http://dx.doi.org/10.1016/j.arabjc.2014.10.043
1878-5352

Catalytic wet air oxidation (CWAO) is known as an effective process to treat high concentrated organic wastewaters, which is too concentrated for practical biological remediation and too dilute for economical incineration and recovery (Gao et al., 2013; Hua et al., 2013; Li et al., 2013; Vallet et al., 2013; Wang et al., 2008). CWAO consists in the total oxidation of the organic species present in effluents to CO_2, N_2 and H_2O under relatively mild conditions of temperature and pressure, using oxygen or air as the oxidizing source, provided that a suitable catalyst is used (Gomes et al., 2008; Parvas et al., 2014). Using proper catalysts for catalytic wet oxidation (CWO) not only reduces the severity of reaction conditions but also decomposes even refractory pollutants (Kim et al., 2009; Mishra et al., 1995). Homogenous transition metals (Fe^{2+}, Cu^{2+}) may be suitable catalysts, but the dissolved ions need to be separated at the end of the process (Besson et al., 2000). Heterogeneous catalysts presenting high activity and stability have been investigated over the years (Arena et al., 2010; Delgado et al., 2012; Kim and Ihm, 2011; Tran et al., 2011; Wei et al., 2013; Yang et al., 2010), since they can be easily removed by filtration from the treated solution (Gomes et al., 2008). Carbon materials, transition metal oxides and CeO_2-based catalysts were also implemented in the CWAO of organic compounds and exhibited good performances (Yang et al., 2010). The advantage of non-noble metal oxide catalysts is their inexpensiveness, but catalytic activity is relatively low. Moreover the active component of non-noble metal catalyst is largely leaching, therefore, non-noble metal catalysts mainly are focused on improving their stability (Jing et al., 2016). Transition metal oxide catalysts are widely studied as an alternative in the CWAO process even if they show rather lower activity than noble metals (Arena et al., 2010; Gomes et al., 2005; Kim et al., 2009). The solution of this problem is using some efficient supports with a better capacity to activate oxygen and facilitating the oxygen transfer from the dissolved phase to the active sites (Kim et al., 2009). TiO_2, CeO_2 and ZrO_2 were proved to be stable and easily available supporting materials (Wang et al., 2008). The addition of ZrO_2 to CeO_2 can improve its oxygen storage capacity, redox properties, thermal resistance and its catalytic activity at low temperatures (Pengpanich et al., 2004). CeO_2–ZrO_2 solid solution with high oxygen mobility is widely applied in exhaust gas purification, removal of organic compounds from wastewaters, reforming of hydrocarbon, and water gas shift reaction (Kambolis et al., 2010; Kim et al., 2009; Pengpanich et al., 2004).

As reported the synthesis method could affect the physicochemical properties of the catalysts (Allahyari et al., 2014; Charghand et al., 2014; Ebrahimynejad et al., 2014). According to the direct effect of the synthesis method on the stability and activity of the catalysts, the sonochemistry method is proposed as a suitable method for settling of metallic nanoparticles on the different supports without damaging to their structure (Khoshbin and Haghighi, 2014; Rahmani et al., 2014b; Sharifi et al., 2014). Ultrasound can enhance and promote dispersion of the active metal on the carrier, thus improving the catalytic performance of the catalyst (Estifaee et al., 2014; Liu et al., 2010; Rahmani et al., 2014a). To the best of our knowledge, the application of ultrasound in the preparation of Ni/CeO_2–ZrO_2 nanocatalyst has not been previously studied.

Therefore in our research, Ni/CeO_2–ZrO_2 nanocatalyst was prepared sonochemically and its structure was examined by XRD, BET, FESEM and FTIR analyses. The performance of this nanocatalyst in the CWAO of phenol was investigated as well. The influence of transition metal content and nanocatalyst loading on phenol conversion were investigated using batch reactor experiments.

2. Materials and methods

2.1. Materials

The following chemicals were employed for the preparation of nanocatalysts: cerium nitrate ($Ce(NO_3)_3{\cdot}6H_2O$; 98.5%) as support precursor, nickel chloride ($NiCl_2{\cdot}6H_2O$; 89%) as active phase precursor, ammonia (NH_3; 33%) as precipitant and phenol (100% purity) as pollutant are purchased from Merck. Zirconium nitrate ($ZrO(NO_3)_2{\cdot}6H_2O$; 99%), as support precursor was purchased from Aldrich.

2.2. Preparation and procedures

The schematic flow chart for the preparation steps of Ni/CeO_2–ZrO_2 nanocatalysts synthesized via co-precipitation and ultrasound assisted methods is shown in Fig. 1. At first (Fig. 1a), the mixed oxide support of CeO_2–ZrO_2 with Ce/Zr molar ratio of 3:1 as support was prepared via co-precipitation method. Appropriate amounts of nitrate salts (cerium nitrate: $Ce(NO_3)_3{\cdot}6H_2O$ and zirconyl nitrate: $ZrO(NO_3)_2{\cdot}2H_2O$) were dissolved in deionized water (Ni: 0%, 5%, 10%, 15%, 20% in catalyst). The precipitate of $Ce(OH)_3$–$Zr(OH)_4$ was obtained by adding aqueous ammonia (28%) drop wise into a mixed aqueous solution at room temperature with stirring until the pH of the mother liquor reached about 9.0. The precipitate was filtered and washed with distilled water, and then dried at 110 °C overnight. Finally, ceria–zirconia mixed oxide was obtained by calcination in air flow at 450 °C for 6 h.

In second stage (Fig. 1b), transition metal (Ni) was put on CeO_2–ZrO_2 loaded by different percentages of active phase (5, 10, 15 and 20 wt%). These nanocatalysts were prepared by the sonochemistry method using an aqueous solution of $NiCl_2.6H_2O$ and the prepared CeO_2–ZrO_2 support. Sonication was carried out on a SONOPULS HD 3200. The slurry irradiated with a high-intensity ultrasonic employing a direct immersion titanium horn of 1 cm^2 (20 kHz, power output 90 W/cm^2) which was inserted 1 cm below the solution, under a flow of argon for 45 min. The sonication flask was fixed in a water bath at room temperature (20–25 °C) during the reaction, whereas the temperature inside the sonication flask was around 60–70 °C. Then, the mixture was dried at 110 °C for 12 h. After drying, the precipitate was calcined in air at a temperature of 500 °C for 5 h.

2.3. Characterizations

The crystal structures of mixed oxide were confirmed by means of a diffractometer SIENENF B5000: Advance-D8 using Cu-Kα radiation. Intensities were obtained in the 2θ range between 20° and 90° with a scanning speed of 0.04° per second. The average crystallite size of nanocatalyst was estimated using the Debye–Scherrer equation:

$$D = \frac{0.90\lambda}{\beta \cos\theta} \quad (1)$$

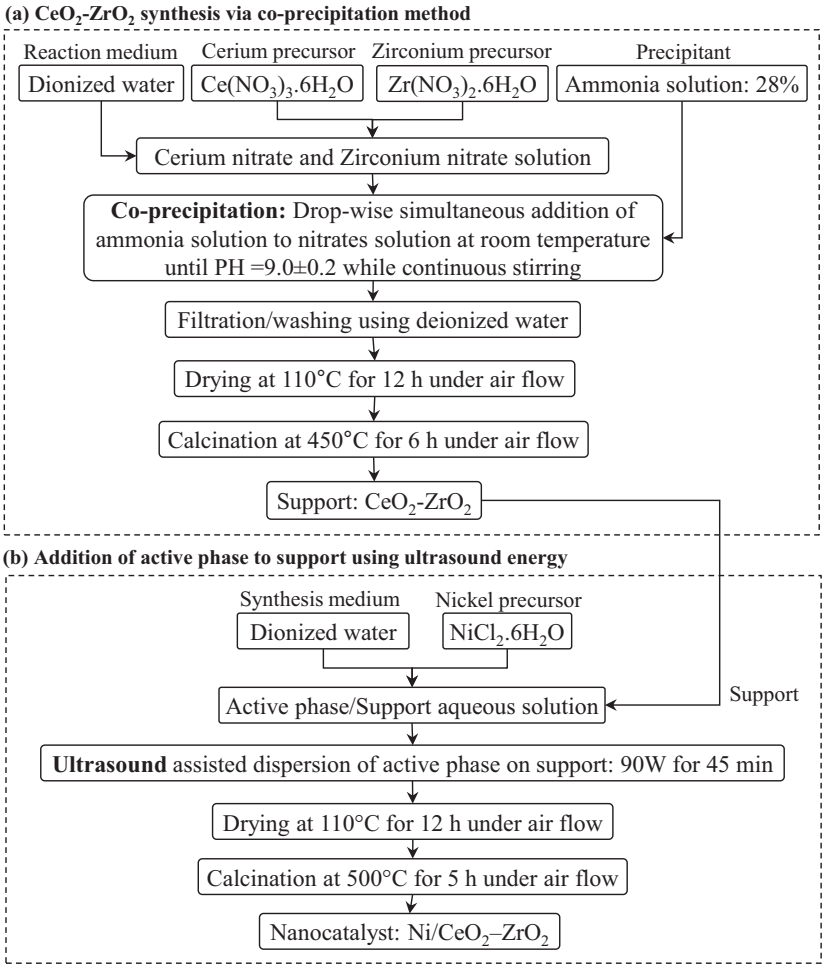

Figure 1 Schematic flow chart for the preparation steps of $Ni/CeO_2–ZrO_2$ nanocatalyst synthesized via co-precipitation and ultrasound assisted methods.

where D is the crystallite size (nm), λ is the wavelength ($\lambda = 0.154056$ nm), β is the corrected full width at half maximum (radian) and θ is the Bragg angle (radian). The samples were characterized at acceleration voltage of 15 kV. Morphology and particle size of the nanocatalysts were observed by Field Emission Scanning Electron Microscopy (FESEM, HITACHI S-4160) analyser. The BET surface area was determined using a CHEMBET-3000 (Quantachorom) apparatus from adsorption of nitrogen at relative pressure between 0.05 and 0.3.

FTIR technique was used at Fourier Transform-Infrared Spectrophotometer (Unicam 4600) to identify the surface functional groups on the nanocatalysts. The samples were characterized at wavelength between 400 and 4000 cm^{-1}.

2.4. Experimental setup for catalytic wet air oxidation

The oxidation experiments were carried out at an atmosphere of O_2 in a 200 ml autoclave equipped with a magnetically driven impeller. The cylinder reactor was made of SS-316 stainless steel. It was equipped with a Teflon liner to prevent severe corrosion problems. A thermal sensor and external heating element are also provided in the reactor for temperature control with an accuracy of ± 1 °C. Typically, in an oxidation run, 100 ml of aqueous solution, containing the pollutant (1000 g/l of phenol) and the desired amount of nanocatalyst powder were loaded inside the cold reactor. After 5 min flushing with O_2, the reactor heated to the reaction temperature. After it was sealed, the reactor was rapidly heated to the desired temperature. Initial O_2 pressure was 1 atm. The operating temperature was chosen to be 160 °C. The mixer was set at 800 rpm to minimize the interfacial mass resistance between the gas and liquid phase and to ensure uniform temperature and concentration profiles in the liquid phase. The nanocatalyst loading in reactor (gr) and active phase loading on support (%) were varied over wide experimental intervals. Once the set temperature was achieved, the time of reaction was initialized and was defined as the start time ($t = 0$). Each run lasted for 3 h. At the end of the reaction, liquid samples were withdrawn, rapidly cooled, centrifuged to remove any catalyst particle in the liquid samples and analyzed. The phenol concentration of each sample was determined using UV–Vis. detector. The UV–Vis. detector was used with a 272 nm wavelength. The conversion of phenol (%) was calculated using the Eq. (2).

$$\text{Phenol conversion } (\%) = \frac{[PhOH]_i - [PhOH]_f}{[PhOH]_i} \times 100 \qquad (2)$$

where $[PhOH]_i$ and $[PhOH]_f$ are the initial and the final concentrations of phenol (mol l^{-1}), respectively.

3. Results and discussions

3.1. Nanocatalysts characterization

3.1.1. XRD analysis

Fig. 2 shows the XRD patterns of CeO_2–ZrO_2 support and Ni/CeO_2–ZrO_2 nanocatalysts with different Ni loadings. The peaks at about 2θ = 37.3°, 43.4°, 63.0°, 75.6° and 79.6° indicated existence of Ni as cubic NiO phase. There is no individual tetragonal ZrO_2 peak. The main CeO_2 peaks (2θ = 28.8°, 33.2°, 47.7°, 56.6°, 59.4°, 69.8°, 77.1°, 79.5° and 88.9°) shifted slightly to higher diffraction angles due to the substitution of the Ce^{4+} atoms (1.09 Å) by the smaller Zr^{4+} atoms (0.86 Å). The crystallite size of CeO_2 and NiO crystals was in the range of 10.4–13.3 nm and 21.4–21.7 nm, respectively, calculated from the X-ray line broadening technique employing the Scherrer equation (Table 1). The peak intensity of NiO became obviously stronger with increasing Ni loading suggesting that at a low Ni loading, NiO was present in the form of small nanoparticles while at a high Ni content, bulk agglomerated particles of NiO were present (Biswas and Kunzru, 2007; Pengpanich et al., 2004).

Fig. 3 demonstrates relative crystallinity of NiO peaks at different Ni contents. With rising in Ni content, a growth in crystallinity of NiO was observed. If the crystallinity of NiO was 100% in 20% wt Ni/CeO_2–ZrO_2, the crystallinity of 5% wt Ni was 41.13%.

3.1.2. FESEM analysis

FESEM micrographs of CeO_2–ZrO_2 support and NiO/CeO_2–ZrO_2 nanocatalysts with different Ni loadings and different magnifications are illustrated in Fig. 4. The CeO_2–ZrO_2 mixed oxide had a uniform morphology with good particle distribution. The CeO_2–ZrO_2 particles were spherical and small in the nanometric range. The introduction of Ni changed the morphology significantly. At 5% wt Ni, a non-uniform morphology was observed. Big agglomeration of particles with irregular shape and size exists in this nanocatalyst. With increasing Ni content, big particles were converted to smaller ones. It seems increasing the Ni active phase content improves the structure of nanocatalyst particles. The particles got

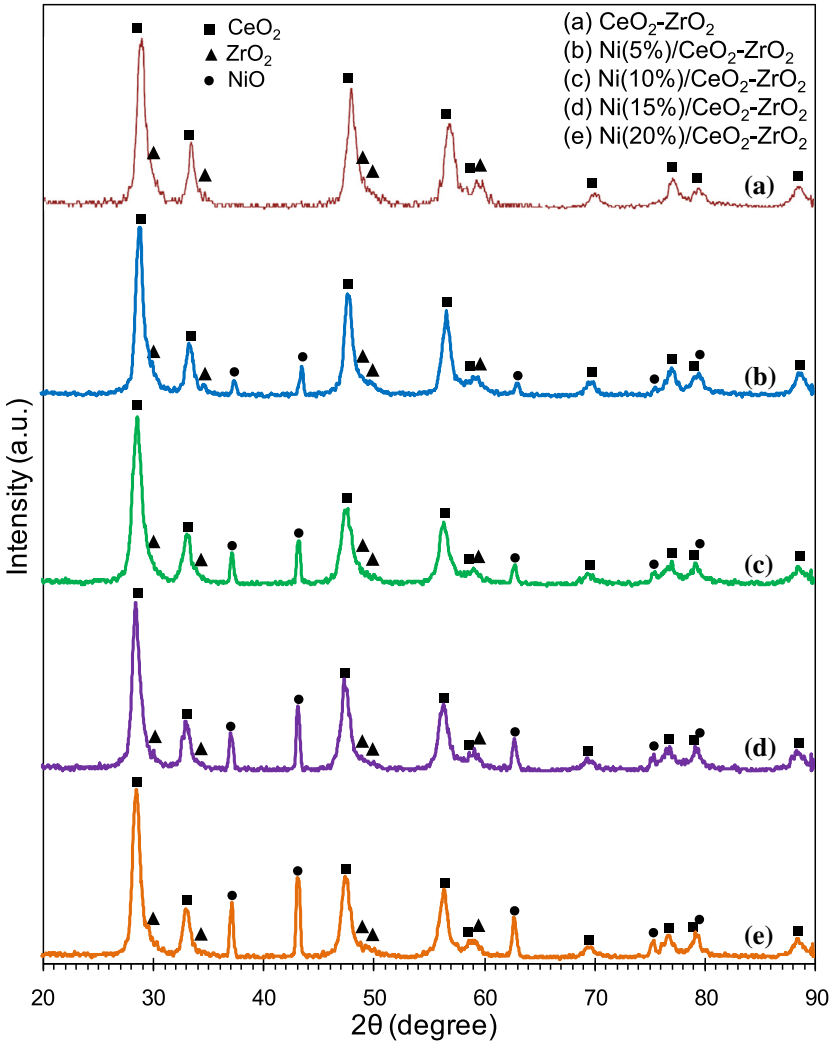

Figure 2 XRD patterns of Ni/CeO_2–ZrO_2 nanocatalysts with different loadings of nickel (a) 0%, (b) 5%, (c) 10%, (d) 15% and (e) 20%.

Table 1 Structural properties of CeO_2–ZrO_2 support and Ni/CeO_2–ZrO_2 nanocatalysts with different loadings of nickel.

Catalyst/support	Ni (wt%)	S_{BET}[a] (m^2/g)	Crystallite size[a] (nm)		
			NiO[b]	CeO_2[c]	ZrO_2[d]
CeO_2–ZrO_2	0	62.7	–	10.4	ND[e]
Ni/CeO_2–ZrO_2	5	26.3	21.7	13.0	ND
Ni/CeO_2–ZrO_2	10	32.7	21.7	10.4	ND
Ni/CeO_2–ZrO_2	15	13.7	21.4	13.3	ND
Ni/CeO_2–ZrO_2	20	24.6	21.5	13.3	ND

[a] Crystallite size estimated by Scherre's equation.
[b] Crystallite phase: cubic, JCPDS number: 01-073-1519.
[c] Crystallite phase: cubic, JCPDS number: 01-075-0076.
[d] Crystallite phase: tetragonal, JCPDS number: 01-080-0784.
[e] Not detected.

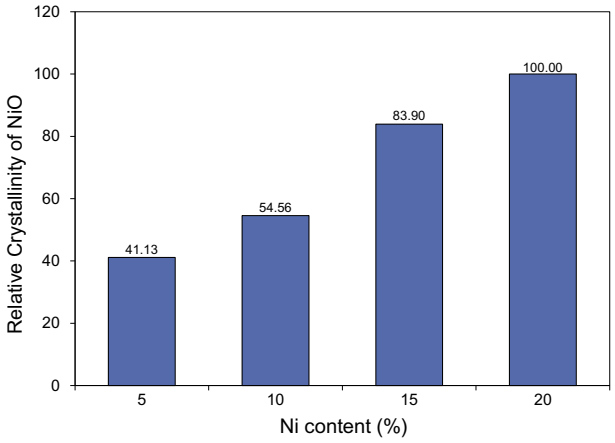

Figure 3 Relative crystallinity of NiO over CeO_2–ZrO_2 with different loadings of nickel.

spherical and a good homogeneity was noticed. The efficiency of the ultrasound was proper and a good nucleation occurred during synthesis that created small and uniform particles. At very loaded Ni content (20% wt), the spherical particles disappeared again. Although the particles in 20% wt Ni were small but distinct clarity in borders of particles did not exist anymore. It seems the concentration of Ni precursor was too high for the applied power of ultrasound; therefore sonication efficiency was not enough for dispersion of Ni particles individually over the support. According to the literature, the agglomerates of particles can be classified as "soft" or "hard", the "hard" agglomerates consisting of close-packed particles with high densities that agglomeration in Ni nanocatalysts is of this kind.

Fig. 5 shows particle size histogram of Ni/CeO_2–ZrO_2 nanocatalyst with 15% loading of nickel. A relatively narrow particle size distribution was observed. The average particle size was 77 nm and 85.71% of particle diameters were less than 100 nm. Considerable amount of particles had sizes in the range of 50–60 nm that shows successful preparation of Ni/CeO_2–ZrO_2 nanocatalyst with the sonochemical method.

3.1.3. BET analysis

Table 1 illustrates the specific BET surface area of the synthesized support and nanocatalysts. The specific surface area of the CeO_2–ZrO_2 support was 62.7 m^2/g. This surface area is comparable to those reported by Biswas and Kunzru (2007) and Liang et al. (2008). After metal addition, a decrease in BET value is observed for CeO_2–ZrO_2 support, presumably due to pore blocking by active metals.

3.1.4. FTIR analysis

Fig. 6 shows the recorded FTIR patterns of CeO_2–ZrO_2 support and NiO/CeO_2–ZrO_2 nanocatalysts with different loadings of transition metal. These figures illustrate the IR spectra of these samples before catalytic reaction. The nanocatalysts displayed infrared absorption bands at 415, 1400 and 1620 cm^{-1}. The characteristic peaks were assigned as follows: The bands at 1400 cm^{-1} are the stretching vibration absorption spectra of H–O. The band at 1625 cm^{-1} is assigned to the deformation vibration mode of the adsorbed water (Abbasi et al., 2011; Pae et al., 2006; Saberi et al., 2008). No peak of chloride precursor has ever appeared in the pattern, which shows that chloride precursor can be completely removed by repeatedly washing with water. Surprisingly no peak at 3450 cm^{-1} was found indicative of hydrogen-bonded O–H species.

The peaks at 415 cm^{-1} corresponds to the metal–oxygen–metal bond (M–O–M) (Saberi et al., 2008). This band can also be related to the stretching vibration absorption spectrum of Ce(Zr)–O. Since this peak changes with increasing Ni content, therefore attribution of this peak to Ni–O–Ni is more likely. This peak got sharper with increasing Ni content that reveals more crystalline structure of NiO at high Ni loadings. This observation is exactly consistent with XRD result.

3.2. Catalytic performance of synthesized nanocatalysts for oxidation of phenol

3.2.1. Effect of different loadings of Ni

Fig. 7 displays effect of active phase loading (Ni) on catalytic performance of Ni/CeO_2–ZrO_2 nanocatalyst. Blank experiments with CeO_2–ZrO_2 proved that the support was weakly active in the oxidation of phenol at 160 °C. Phenol conversion stabilized around 11.4% with 0% Ni. It can be seen that the doping of Ni species on the CeO_2–ZrO_2 improved catalytic activity for CWAO of phenol. Phenol conversion increased with the increase of active phase. The active phase dispersion on the support might vary as a function of the active phase loading and the catalytic performances might be consequently affected. After 3 h reaction, the phenol conversions were

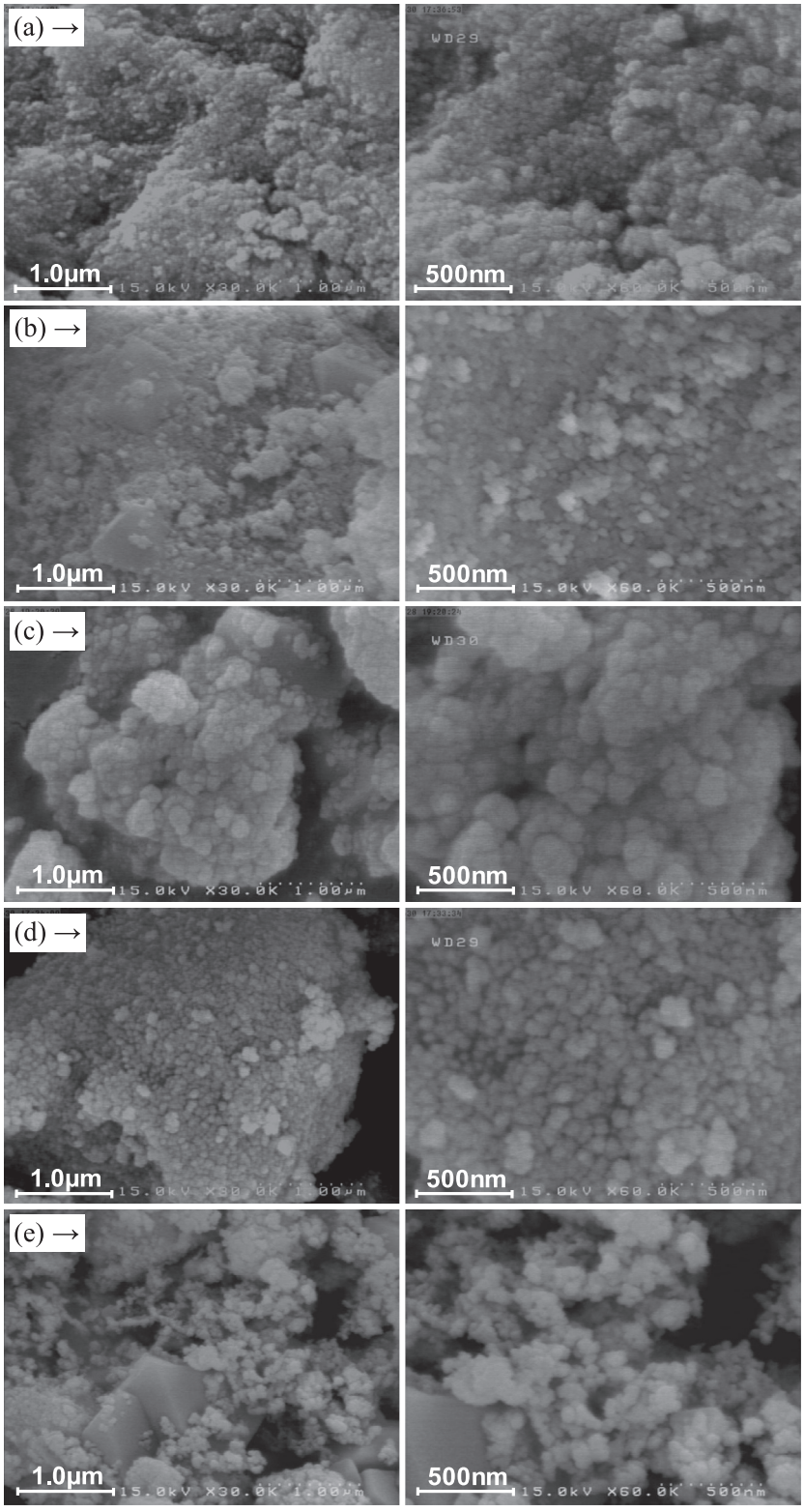

Figure 4 FESEM images of $Ni/CeO_2–ZrO_2$ nanocatalysts with different loadings of nickel (a) 0%, (b) 5%, (c) 10%, (d) 15% and (e) 20%.

29.5% over 20wt % Ni nanocatalyst. Phenol removal percent did not noticeably change with increasing Ni content from 15% to 20% wt. According to FESEM micrographs of attributed samples, appearance of agglomerated particles in 20% wt Ni sample, lowered the available active sites and declined the catalyst reactivity in this case.

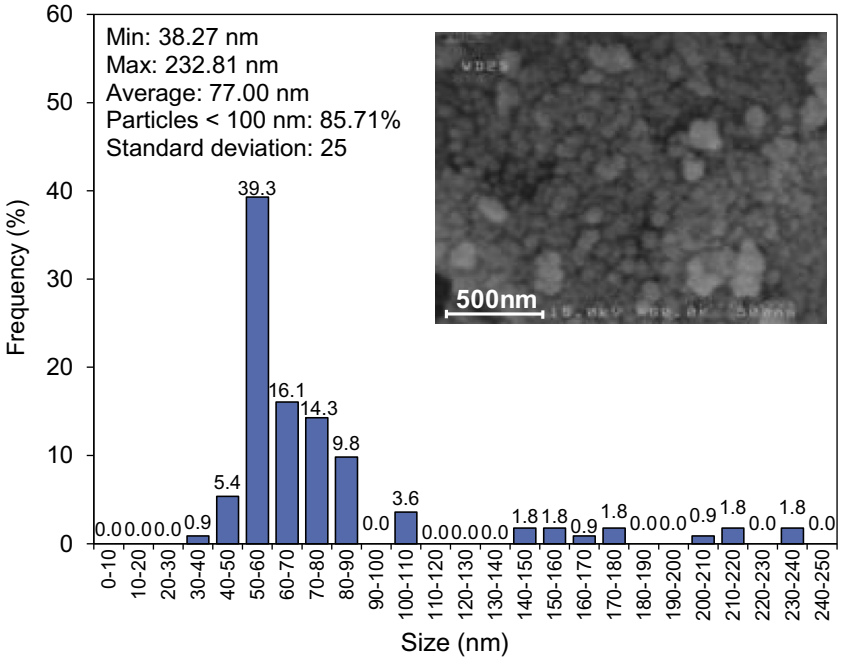

Figure 5 Particle size histogram of $Ni/CeO_2–ZrO_2$ nanocatalyst with 15% loading of nickel.

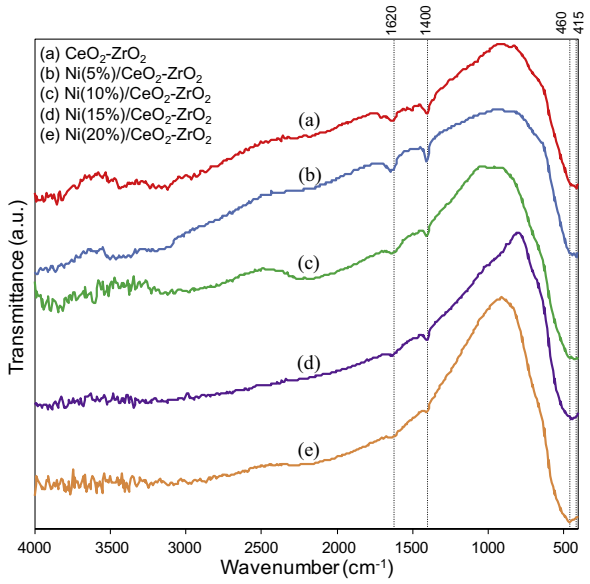

Figure 6 FTIR spectrum of $Ni/CeO_2–ZrO_2$ nanocatalysts with different loadings of nickel (a) 0%, (b) 5%, (c) 10%, (d) 15% and (e) 20%.

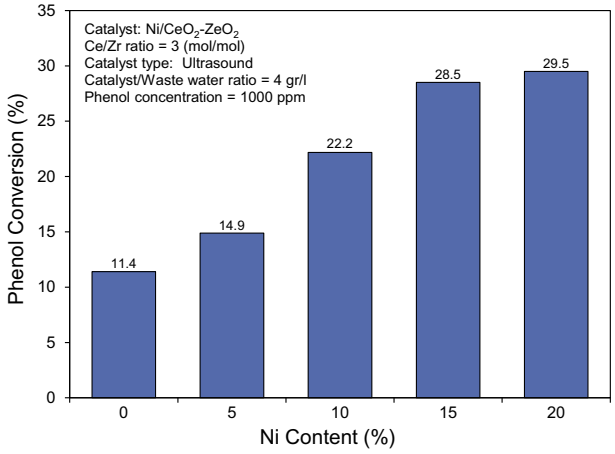

Figure 7 Effect of different loadings of active components (Cu and Ni) on catalytic performance of $Ni/CeO_2–ZrO_2$ nanocatalysts for phenol conversion.

3.2.2. Effect of nanocatalyst loading

The effect of catalyst loading on the activity of NiO(15wt%)/$CeO_2–ZrO_2$ is illustrated in Fig. 8. Nanocatalyst loading is one of the important parameters in kinetics of chemical reactions. We have found that the efficiency of CWAO of phenol increased with nanocatalyst loading from 1.0 to 9.0 g/l, but decreased when the loading was increased to 10.0 g/l. Higher nanocatalyst loadings correspond to higher active sites and it is expected to increase the removal of phenol, however, as can be seen, an optimum phenol removal at 9.0 g/l of nanocatalyst loading exists. Therefore, increasing the nanocatalyst loading did not necessarily increase the phenol removal. In fact, higher nanocatalyst loading may cause mass transfer limitations and on the other hand some parts of nanocatalysts may not incorporate in the reaction.

3.3. Reaction network of phenol oxidation over synthesized nanocatalysts

The catalytic wet air oxidation of organics is widely acknowledged to proceed via a free-radical chain reaction mechanism (Chang et al., 2003; Lin et al., 2003; Lin and Weng, 1994; Rivas et al., 1998) and the condition of stationary free radical concentration is usually assumed (Chang et al., 2002; Lin and

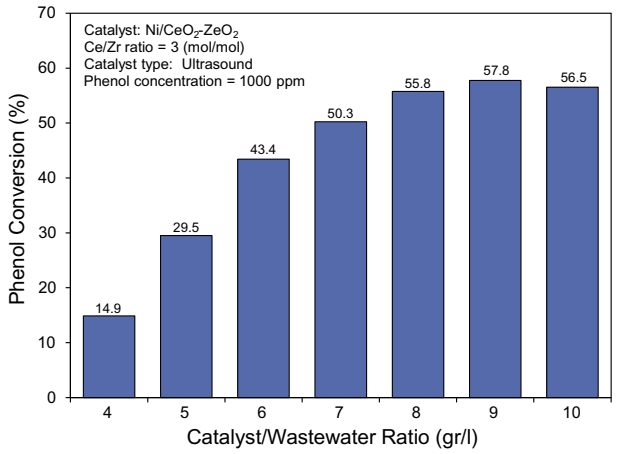

Figure 8 Effect of catalyst loading on the catalytic performance of $Ni/CeO_2–ZrO_2$ nanocatalysts for phenol conversion.

Weng, 1993). The critical nanocatalyst concentration phenomenon as observed in this work, is one of the characteristics of free radical chain reaction, in which a slight change in nanocatalyst loading (active phase loading and nanocatalyst loading in reactor) induces a noticeable change in the rate of process (Sadana, 1979). According to this mechanism, the nanocatalyst simultaneously plays dual roles of initiator and terminator of free radicals. The rate of free radical formation is dependent on the amount of active sites over the nanocatalyst. The amount of active sites varies with transition metal content and/or nanocatalyst loading. Because the free radicals are initially induced by nanocatalyst, hence the rate of free radical formation, as well as the rate of phenol conversion, will increase as the nanocatalyst loading is increased. Besides, the rate of free radical formation competes with the rate of free radical destruction and both the formation rate and the destruction rate increase with nanocatalyst loading. The solid nanocatalyst simultaneously plays the role of terminator for free radicals as well. Thus the destruction rate of free radicals increases with nanocatalyst loading, too. However, at a lower nanocatalyst loading (9.0 g/l), free radical formation is higher, while at a higher loading (10.0 g/l), free radical destruction dominates. Hence there exists an optimal loading (Chang et al., 2005; Lin et al., 2003).

A reaction undergoing free radical mechanism consists of initiation, propagation and termination periods. The electron is first transferred from nanocatalyst to phenol to initiate the free radicals. Then the free radicals are propagated by reacting with phenol and oxygen. Finally, free radicals are terminated by colliding with each other (Wu et al., 2003). The redox potential of the Ce^{4+}/Ce^{3+} couple is a main factor to promote the oxidation. Substitution of the Ce^{4+} atoms by the smaller Zr^{4+} atoms in $CeO_2–ZrO_2$ mixed oxide reduces the redox potential. So electron transfer between Ce^{4+} and Ce^{3+} will be easier and therefore oxygen transfer will be faster. As can be seen in Fig. 9 the role of $CeO_2–ZrO_2$ mixed oxide support in free radical mechanism of phenol wet air oxidation was ascribed to be in the activation of phenol molecule and oxygen. $CeO_2–ZrO_2$ mixed oxide support allows a fast initial degradation of phenol into intermediate products, followed by a slow oxidation of the intermediate compounds into low molecular weight organic acids, CO_2 and water. Ni has a similar role in the activation of phenol and oxygen also because after introduction of Ni to the support, the amount of phenol degradation increased (see Section 3.2.1). Although Ni can accelerate oxygen transfer via Ni^{+2}/Ni^{+1} redox but produced free radicals because of $CeO_2–ZrO_2$ mixed oxide will be captured by Ni particles as well. Another role of Ni may be the enhancement of the rate of oxidation of small organic compounds that are resistant and not easily degraded by the $CeO_2–ZrO_2$ mixed oxide support (Gallezot et al., 1997; Jr et al., 1998). According to less favorable Ni^{+2}/Ni^{+1} redox potential, we assume latter role is more dominant in mineralization of phenol to CO_2 and H_2.

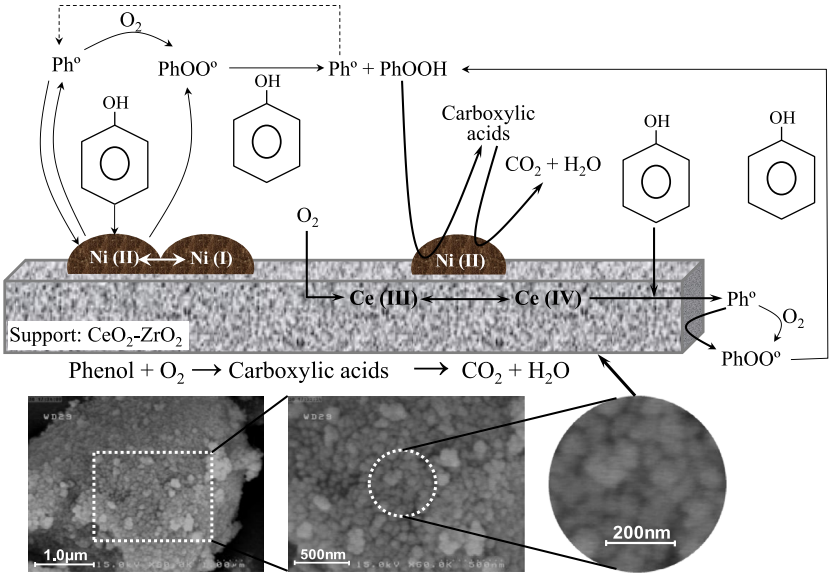

Figure 9 Simplified reaction pathway for CWAO of phenol over synthesized $Ni/CeO_2–ZrO_2$ nanocatalysts.

4. Conclusions

The main findings of this study can be summarized as follows:

- According to XRD, existence of CeO_2–ZrO_2 mixed oxide in Ni/CeO_2–ZrO_2 nanocatalyst was confirmed.
- In Ni/CeO_2–ZrO_2 nanocatalyst, Ni existed as NiO and while the crystallinity of NiO enhanced with rising in Ni content, the size of NiO crystals did not significantly change.
- Big agglomeration of particles with irregular shape and size was observed in the nanocatalyst with lower Ni contents. With increasing Ni content, big agglomerated particles converted to smaller particles and the structure of nanocatalyst particles improved.
- The IR peaks attributed to Ni–O–Ni, got sharper with increasing Ni content that reveals more crystalline structure of NiO at high Ni loadings, consistent with XRD result.
- Doping of Ni on the CeO_2–ZrO_2 mixed oxide improved catalytic activity for CWAO of phenol and its conversion increased with the rising of active phase content.
- There was an optimum in removal of phenol at 9.0 g/l of nanocatalyst loading that means increasing the nanocatalyst loading not necessarily increases the phenol removal.
- A reaction pathway was proposed for CWAO of phenol based on dual role for Ni: activating of phenol and oxygen (similar to role of CeO_2–ZrO_2 support) and converting of refractory intermediates produced over CeO_2–ZrO_2 support.

Acknowledgments

The authors gratefully acknowledge Sahand University of Technology for the financial support of the project as well as Tabriz Oil Refining Company and Iran Nanotechnology Initiative Council for complementary financial support.

References

Abbasi, Z., Haghighi, M., Fatehifar, E., Saedy, S., 2011. Synthesis and physicochemical characterizations of nanostructured Pt/Al_2O_3–CeO_2 catalysts for total oxidation of VOCs. J. Hazard. Mater. 186, 1445–1454.

Allahyari, S., Haghighi, M., Ebadi, A., Qavam Saeedi, H., 2014. Direct synthesis of dimethyl ether as a green fuel from Syngas over nanostructured CuO–ZnO–Al_2O_3/HZSM-5 catalyst: influence of irradiation time on nanocatalyst properties and catalytic performance. J. Power Sources 272, 929–939.

Arena, F., Italiano, C., Raneri, A., Saja, C., 2010. Mechanistic and kinetic insights into the wet air oxidation of phenol with oxygen (CWAO) by homogeneous and heterogeneous transition-metal catalysts. Appl. Catal., B 99, 321–328.

Besson, M., Beziat, J.-C., Blanc, B., Durecu, S., Gallezot, P., 2000. Treatment of aqueous solutions of organic pollutants by heterogeneous catalytic wet air oxidation (CWAO). Stud. Surf. Sci. Catal. 130, 1553–1558.

Biswas, P., Kunzru, D., 2007. Steam reforming of ethanol for production of hydrogen over Ni/CeO_2–ZrO_2 catalyst: effect of support and metal loading. Int. J. Hydrogen Energy 32, 969–980.

Chang, D.J., Chen, I.P., Chen, M.T., Lin, S.S., 2003. Wet air oxidation of a reactive dye solution using CoAlPO_4-5 and CeO_2 catalysts. Chemosphere 52, 943–949.

Chang, D.J., Lin, S.S., Chen, C.L., Wang, S.P., Ho, W.L., 2002. Catalytic wet air oxidation of phenol using CeO_2 as the catalyst – kinetic study and mechanism development. J. Environ. Sci. Health Part A 37, 1241–1252.

Chang, L., Chen, I.-P., Lin, S.-S., 2005. An assessment of the suitable operating conditions for the CeO_2/Al_2O_3 catalyzed wet air oxidation of phenol. Chemosphere 58, 485–492.

Charghand, M., Haghighi, M., Aghamohammadi, S., 2014. The beneficial use of ultrasound in synthesis of nanostructured Ce-doped SAPO-34 used in methanol conversion to light olefins. Ultrason. Sonochem. 21, 1827–1838.

Delgado, J.J., Chen, X., Perez-Omil, J.A., Rodriguez-Izquierdo, J.M., Cauqui, M.A., 2012. The effect of reaction conditions on the apparent deactivation of Ce–Zr mixed oxides for the catalytic wet oxidation of phenol. Catal. Today 180, 25–33.

Ebrahimynejad, M., Haghighi, M., Asgari, N., 2014. Ultrasound assisted synthesis and physicochemical characterization of fluorine-modified CoMo/Al_2O_3 nanocatalysts used for hydrodesulfurization of thiophene. J. Nanosci. Nanotechnol. 14, 6848–6857.

Estifaee, P., Haghighi, M., Mohammadi, N., Rahmani, F., 2014. CO oxidation over sonochemically synthesized Pd–Cu/Al_2O_3 nanocatalyst used in hydrogen purification: effect of Pd loading and ultrasound irradiation time. Ultrason. Sonochem. 21, 1155–1165.

Gallezot, P., Chaumet, S., Perrard, A., Isnard, P., 1997. Catalytic wet air oxidation of acetic acid on carbon-supported ruthenium catalysts. J. Catal. 168, 104–109.

Gao, P., Li, N., Wang, A., Wang, X., Zhang, T., 2013. Perovskite $LaMnO_3$ hollow nanospheres: the synthesis and the application in catalytic wet air oxidation of phenol. Mater. Lett. 92, 173–176.

Gomes, H.T., Machado, B.F., Ribeiro, A., Moreira, I., Rosario, M., Silva, A.M.T., Figueiredo, J.L., Faria, J.L., 2008. Catalytic properties of carbon materials for wet oxidation of aniline. J. Hazard. Mater. 159, 420–426.

Gomes, H.T., Selvam, P., Dapurkar, S.E., Figueiredo, J.L., Faria, J.L., 2005. Transition metal (Cu, Cr, and V) modified MCM-41 for the catalytic wet air oxidation of aniline. Microporous Mesoporous Mater. 86, 287–294.

Hua, L., Ma, H., Zhang, L., 2013. Degradation process analysis of the azo dyes by catalytic wet air oxidation with catalyst CuO/γ-Al_2O_3. Chemosphere 90, 143–149.

Jing, G., Luan, M., Chen, T., 2016. Progress of catalytic wet air oxidation technology. Arab. J. Chem. 9 S1208–S1213.

Jr, J.B., Delanoë, F., Jabouille, F., Blanchard, G., Isnard, P., 1998. Total oxidation of acetic acid in aqueous solutions over noble metal catalysts. J. Catal. 177, 378–385.

Kambolis, A., Matralis, H., Trovarelli, A., Papadopoulou, C., 2010. Ni/CeO_2–ZrO_2 catalysts for the dry reforming of methane. Appl. Catal., A 377, 16–26.

Khoshbin, R., Haghighi, M., 2014. Direct conversion of syngas to dimethyl ether as a green fuel over ultrasound-assisted synthesized CuO–ZnO–Al_2O_3/HZSM-5 nanocatalyst: effect of active phase ratio on physicochemical and catalytic properties at different process conditions. Catal. Sci. Technol. 4, 1779–1792.

Kim, K.-H., Ihm, S.-K., 2011. Heterogeneous catalytic wet air oxidation of refractory organic pollutants in industrial wastewaters: a review. J. Hazard. Mater. 186, 16–34.

Kim, K.-H., Kim, J.-R., Ihm, S.-K., 2009. Wet oxidation of phenol over transition metal oxide catalysts supported on $Ce_{0.65}Zr_{0.35}O_2$ prepared by continuous hydrothermal synthesis in supercritical water. J. Hazard. Mater. 167, 1158–1162.

Li, Y., Zhang, F., Liang, X., Yediler, A., 2013. Chemical and toxicological evaluation of an emerging pollutant (enrofloxacin) by catalytic wet air oxidation and ozonation in aqueous solution. Chemosphere 90, 284–291.

Liang, Q., Wu, X., Weng, D., Lu, Z., 2008. Selective oxidation of soot over Cu doped ceria/ceria–zirconia catalysts. Catal. Commun. 9, 202–206.

Lin, S.S., Chang, D.J., Wang, C.-H., Chen, C.C., 2003. Catalytic wet air oxidation of phenol by CeO_2 catalyst – effect of reaction conditions. Water Res. 37, 793–800.

Lin, S.S., Weng, H.S., 1993. Liquid-phase oxidation of cyclohexane using CoAPO-5 as the catalyst. Appl. Catal., A 105, 289–308.

Lin, S.S., Weng, H.S., 1994. Liquid-phase oxidation of cyclohexane over CoAPO-5: synergism effect of coreactant and solvent effect. Appl. Catal., A 118, 21–31.

Liu, H., Zhang, S., Zhou, Y., Zhang, Y., Bai, L., Huang, L., 2010. Effect of ultrasonic irradiation on the catalytic performance of PtSnNa/ZSM-5 catalyst for propane dehydrogenation. Ultrason. Sonochem..

Mishra, V.S., Mahajani, V.V., Joshi, J.B., 1995. Wet air oxidation. Ind. Eng. Chem. Res. 34, 309–326.

Pae, Y.I., Shin, D.C., Sohn, J.R., 2006. CeO_2-promoted highly active catalyst, $NiSO4/CeO_2–ZrO_2$ for ethylene dimerization. Bull. Korean Chem. Soc. 27, 1989–1996.

Parvas, M., Haghighi, M., Allahyari, S., 2014. Degradation of phenol via wet-air oxidation over $CuO/CeO_2–ZrO_2$ nanocatalyst synthesized employing ultrasound energy: physicochemical characterization and catalytic performance. Environ. Technol. 35, 1140–1149.

Pengpanich, S., Meeyoo, V., Rirksomboon, T., 2004. Methane partial oxidation over $Ni/CeO_2–ZrO_2$ mixed oxide solid solution catalysts. Catal. Today 93–95, 95–105.

Pintar, A., Levec, J., 1994. Catalytic liquid-phase oxidation of phenol aqueous solutions. A kinetic investigation. Ind. Eng. Chem. Res. 33, 3070–3077.

Rahmani, F., Haghighi, M., Estifaee, P., 2014a. Synthesis and characterization of $Pt/Al_2O_3–CeO_2$ nanocatalyst used for toluene abatement from waste gas streams at low temperature: conventional vs. plasma–ultrasound hybrid synthesis methods. Microporous Mesoporous Mater. 185, 213–223.

Rahmani, F., Haghighi, M., Vafaeian, Y., Estifaee, P., 2014b. Hydrogen production via CO2 reforming of methane over ZrO_2-doped Ni/ZSM-5 nanostructured catalyst prepared by ultrasound assisted sequential impregnation method. J. Power Sources 272, 816–827.

Rivas, F.J., Kolaczkowski, S.T., Beltran, F.J., McLurgh, D.B., 1998. Development of a model for the wet air oxidation of phenol based on a free radical mechanism. Chem. Eng. Sci. 53, 2575–2586.

Saberi, A., Golestani-Fard, F., Sarpoolaky, H., Willert-Porada, M., Gerdes, T., Simon, R., 2008. Chemical synthesis of nanocrystalline magnesium aluminate spinel via nitrate–citrate combustion route. J. Alloys Compd. 462, 142–146.

Sadana, A., 1979. Analysis of heterogeneously catalyzed free-radical oxidation of phenol in aqueous-solution. Ind. Eng. Chem. Process Des. Dev. 18, 50–56.

Sharifi, M., Haghighi, M., Abdollahifar, M., 2014. Hydrogen production via reforming of biogas over nanostructured Ni/Y catalyst: effect of ultrasound irradiation and Ni-content on catalyst properties and performance. Mater. Res. Bull. 60, 328–340.

Tran, N.D., Besson, M.I., Descorme, C., Fajerwerg, K., Louis, C., 2011. Influence of the pretreatment conditions on the performances of CeO_2-supported gold catalysts in the catalytic wet air oxidation of carboxylic acids. Catal. Commun. 16, 98–102.

Vallet, A., Ovejero, G., Rodríguez, A., Peres, J.A., García, J., 2013. Ni/MgAlO regeneration for catalytic wet air oxidation of an azo-dye in trickle-bed reaction. J. Hazard. Mater. 244–245, 46–53.

Wang, J., Zhu, W., Yang, S., Wang, W., Zhou, Y., 2008. Catalytic wet air oxidation of phenol with pelletized ruthenium catalysts. Appl. Catal., B 78, 30–37.

Wei, H., Yan, X., He, S., Sun, C., 2013. Catalytic wet air oxidation of pentachlorophenol over Ru/ZrO_2 and Ru/ZrSiO2 catalysts. Catal. Today 201, 49–56.

Wu, Q., Hu, X., Yue, P.-L., 2003. Kinetics study on catalytic wet air oxidation of phenol. Chem. Eng. Sci. 58, 923–928.

Yang, S., Besson, M., Descorme, C., 2010. Catalytic wet air oxidation of formic acid over $Pt/Ce_xZr_{1-x}O_2$ catalysts at low temperature and atmospheric pressure. Appl. Catal., B 100, 282–288.